The Astronomical Journal, 164:47 (10pp), 2022 August https://doi.org/10.3847/1538-3881/ac7561


# The All-sky Spectrometer of Hot Cosmic Plasma

Zh. T. Kambarova[1], A. O. Saulebekov[2], and A. A. Trubitsyn[3]
[1] Buketov Karaganda University, Universitetskaya Street, 28, Karaganda, 100026, Kazakhstan; kambarova@bk.ru
[2] Lomonosov Moscow State University, Kazakhstan branch, Kajimukan Street, 11, Nur-Sultan,010010, Kazakhstan
[3] Ryazan State Radio Engineering University named after V.F. Utkin, Gagarina Street, 59/1, Ryazan, 390005, Russia
*Received 2022 January 20; revised 2022 April 28; accepted 2022 May 31; published 2022 July 12*

## Abstract

The main instruments for analyzing the processes occurring in cosmic plasma are energy and mass analyzers of charged particle beams. The analyzers' operation is based on the separation of charged particles according to the energies of their motion or their masses in electric or magnetic fields. Currently, the top-hat analyzer is considered the main instrument for obtaining information about the state of cosmic plasma. However, it has a number of disadvantages: a significant time cycle for registering angular dependences in a total solid angle of $4\pi$ sr and low accuracy of determining the polar angles, which are associated with the need to rotate the analyzer during measurements. Over the past 20 years, plasma analyzers with a large viewing angle have been developed as an alternative to the top-hat analyzer. The design of the analyzer proposed in this work is capable of measuring plasma characteristics in a solid angle of $2\pi$ sr in one act of data registration. The all-sky spectrometer of hot cosmic plasma consists of two stages: the first stage is a conical lens of an original design, which serves to transform an extremely wide entrance flow of particles into a narrow cone-shaped beam; the second hexapole-cylindrical stage plays the role of an energy analyzer of a narrow cone-shaped flow. The paper describes the calculations and modeling of the proposed analyzer on the basis of original numerical and approximate analytical methods for designing systems of electron and ion optics. The main parameters of the device are calculated.

*Unified Astronomy Thesaurus concepts:* Spectrometers (1554); Space plasmas (1544)

## 1. Introduction

The objects of research in the field of space plasma physics are the radiation belts of the Earth (South Atlantic Anomaly), the solar wind, the collisionless shock wave of the Earth's magnetosphere, the tail of the magnetosphere, the polar lights, the kilometric radiation of the Earth, etc. These studies, in particular, include the study of such characteristics of the hot plasma distribution as the ionic composition, the shape of the energy spectra and angular distributions, as well as the determination of its structure and the nature of the processes occurring in it.

The instruments predominantly used for studying hot space plasma are energy and mass analyzers of charged particle beams—ions and electrons with energies from a few eV to tens of keV. Energy and mass analysis of moving particles is carried out by spatially separating them in electric and magnetic fields. In terms of mass-dimensional indicators, devices with electrostatic deflection of charged particles are out of competition. An additional parameter that needs to be measured during research in space is the direction of arrival of particles. The purpose of measurements of the mass, energy, and angular dependences of ion flows is to map the distribution of charged particles (of plasma).

Devices for the simultaneous angular and energy analysis of cosmic plasma have passed through several stages in their development. In the initial stages of the engineering development, simple single-channel spectrometers (Neugebauer & Snyder 1962), or combinations of them, were used to measure the three-dimensional velocity distribution function. The next step in their progress is the development of a spectrographic method for registration of charged particles. In the design of the spectrograph (O'Brien et al. 1967), a pair of plates was used that ensured the dispersion of particle flows with respect to energy, which made it possible to simultaneously register electrons and ions of various energies using a line of detectors. The use of quarter-spherical and hemispherical analyzers with a knife-edge field of view, the acceptance angle (for particle reception) of which reached 140°–160° (Wolfe et al. 1966), can be considered the next achievement of space plasma diagnostic methods.

The "main tool" of space research today is rightly considered the axially symmetric top-hat analyzer (Paschmann et al. 1985), which is selective in terms of kinetic energy $E$ and the direction of motion of charged particles. The selection of particles by energy is provided by a pair of concentric hemispherical electrodes: a grounded outer hemisphere and an inner hemisphere with a deflecting potential $V$. Two parallel, closely spaced disks of a sufficiently large radius are located at the top of the outer hemisphere parallel to the base of the hemispheres; the polar angle $\theta = 90°$ of motion of the registered particles in a spherical coordinate system is fixed. By gradually changing the potential $V$ of the inner hemisphere, one can scan the entire spectrum of energies $E$ of charged particles. Registration of the particle distribution by azimuth angle $\varphi$ is ensured by using a plane position-sensitive detector as a collector, since a particle with a certain angle $\phi$ is displayed as a single point on the circumference of the entire image. Measurement of the distribution function of charged particles in the entire range of $4\pi$ sr is provided for half the period of rotation of the satellite around its axis.

The top-hat analyzer is successfully used to investigate key regions of the electromagnetic plasma, not only of the Earth,

but also of other planets of the solar system (Machida et al. 1998).

The top-hat analyzer is still the focus of interest of many developers of devices for diagnostics of cosmic plasma, who propose ways to improve its parameters (Kazama 2013; Collinson et al. 2018; Li et al. 2018) and study the influence of various external factors on the main characteristics of the device (Allegrini et al. 2016).

The scope of the top-hat analyzer is constantly expanding. In particular, with its help, the plumes of charged particles generated by an ion engine in the far field are investigated by Victor et al. (2006). The work by Fernandes & Lynch (2016) presents the results of observation of low-altitude ionospheric origins of high-latitude ion upflow/outflow. The main measurement problem, which was resolved within the framework of the created theoretical model, was the extremely low energy (tenths of an eV) of ions at an altitude of 200–350 km.

The disadvantage of the top-hat analyzer is the significant time cycle for registration of the angular dependences in the total solid angle of $4\pi$ sr and low accuracy in determining the polar angles due to the principle of mechanical displacement (rotation) underlying the measurements.

Over the past 20 years, plasma analyzers with a large field of view have been continuously developed, including those based on a top-hat analyzer with entrance optics, which allows the polar angles $\theta$ to be scanned in a rather wide range (Collinson et al. 2016).

A good example of plasma analysis systems built on schemes other than top-hat is the Fast Imaging Plasma Spectrometer (FIPS; Andrews et al. 2007), a simplified scheme of which has proven itself well in the flight of the "Messenger" interplanetary probe and has shown that it really is not only an alternative to the top-hat, but also allows one to carry out unique measurements in various plasma environments. The FIPS energy and mass analyzer with a field of view of almost $2\pi$ sr consists of a wide-angle two-chamber electrostatic analyzer that forms an image of the angular distribution of ions on a multibeam collimator located in front of the time-of-flight (TOF) camera.

In parallel, more efficient $2\pi$ or $4\pi$ systems were being developed, which will probably soon be mounted on spacecraft.

O. L. Vaisberg proposed and investigated a new method for the simultaneous measurement of the velocity vector of charged particles in a solid angle of $2\pi$ sr (Vaisberg 2003). The scheme (Figure 1) of a complete view of the celestial hemisphere is based on the transmission of a particle flow (1), emitted by sources (2) distributed in a certain way in space, through a ring diaphragm (3). Due to the design characteristics of the device, the range of entrance angles in each meridian section is divided into two subranges from $-90°$ to $0°$ and from $0°$ to $+90°$ relative to the axis of symmetry $0z$. In this geometry, only a hemisphere section of radius $r_0$, which is an infinitesimal value with respect to the radius of the virtual celestial sphere, is excluded from consideration. Further, a wide entrance flow of charged particles is converted into a narrow collimated one, subjected to energy analysis, and detected by a position-sensitive detector, with each coordinate on the detector plane being associated with the direction to the source on the celestial hemisphere.

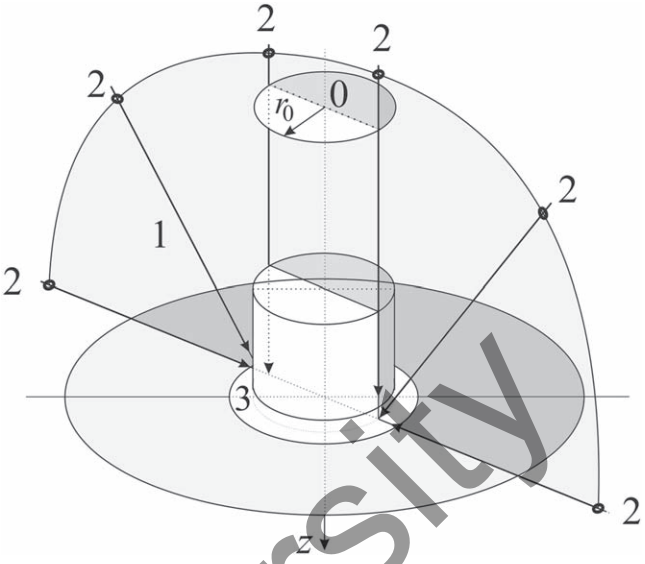


**Figure 1.** Entrance of particles into the particle analysis device: 1—particle flow, 2—sources of particles distributed on the virtual celestial sphere, 3—entrance ring diaphragm.

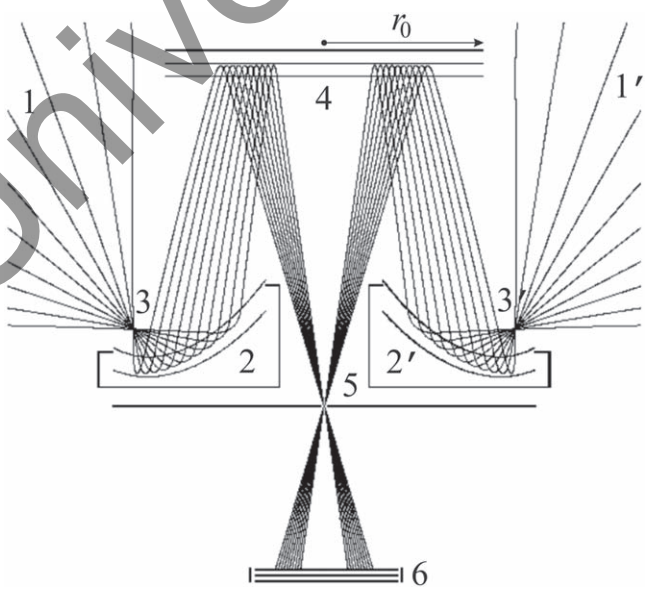


**Figure 2.** Meridian section of the "CAMera" analyzer: 1–1′—particle flow, 2–2′—main elliptical mirror, 3–3′—entrance ring diaphragm, 4—secondary plane mirror, 5—exit point diaphragm, 6—position-sensitive detector.

Figure 2 shows the electron-optical scheme of a device for the simultaneous energy and angular analysis of charged particle flows in a solid angle of $2\pi$ sr, called "CAMera" (Vaisberg 2003). Particle flow (1) enters the main electrostatic elliptical mirror (2) through the ring aperture (3) and is reflected by the mirror into a narrow collimated beam. The selection of energy, or energy scanning, is carried out using a secondary plane mirror (4). A point diaphragm (5) cuts particles with the energy of analyzer settings (4) out from the flow, the particles being recorded by the position-sensitive detector (6). Note the fact that each charged particle moving in the analyzer intersects the plane of the grid electrodes four times, and one of these electrodes has a complex geometric shape.

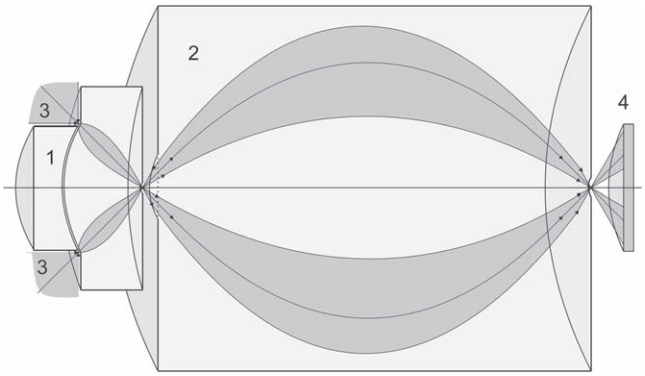


**Figure 3.** The scheme explaining the idea of the developed all-sky spectrometer: 1—the first stage of converting a wide ion flow into a narrow cone-shaped one, 2—the dispersive energy analyzer, 3—an ion flow, 4—a position-sensitive detector.

The successful development and testing of plasma analyzers DI-Aries (DI is for Sensor of Ions in Russian and Aries for the constellation of the zodiac; Vaisberg et al. 2010) and PICAM (Planetary Ion Camera; Vaisberg et al. 2006; Becker 2013) have confirmed a new concept based on rotationally symmetric electrostatic mirrors for the creation of ion analyzers with an instant half-spatial overview field. At each step of energy measurement, ion optics provides a two-dimensional image of the angles of ion motion on a microchannel detector with high time resolution and acceptable angular resolution. Current and future research will mainly focus on increasing the geometric factor of the device and achieving a simpler and more accurate mechanical design (Vaisberg et al. 2016).

The disadvantages of analyzers of the "CAMera" type are a large number of grids and technological difficulties in the manufacture of elliptical grid mirrors. The purpose of this research is to develop a simplified energy analyzer design with a minimum number of grids to provide a $2\pi$ view of the celestial sphere.

## 2. The Idea of the Proposed Spectrometer

The idea of the analyzer design proposed in this work is to use distributed fields created by devices of simple design. The scheme of an axially symmetric device in the most general form is shown in Figure 3. The device consists of two stages: 1 and 2. Stage 1 is designed to convert a wide ion flow 3 with a range of polar angles from 0° to 90° (see the diagram in Figure 1) into a narrow cone-shaped flow directed to the entrance of stage 2. Stage 2 plays the role of a dispersive energy analyzer, in which ions are detected by a plane position-sensitive detector (see the diagram in Figure 2). We emphasize once again that in the developed device it is proposed to use distributed electrostatic fields, the refractive index of which changes continuously, in contrast to fields concentrated in space, created by grid electrodes, as in the CAMera scheme (Figure 2). Note that in electron optics, distributed fields are mainly used due to the stability of optical parameters to manufacturing errors and various external influences on design. In this work, the main tool for developing the design of the device and its stages was the software for numerical modeling of electron optics systems CAE "Focus" (Trubitsyn et al. 2017). Part of the study was carried out using approximate analytical methods for the synthesis of electrostatic fields for energy analysis of charged particle beams (Gurov et al. 2015).

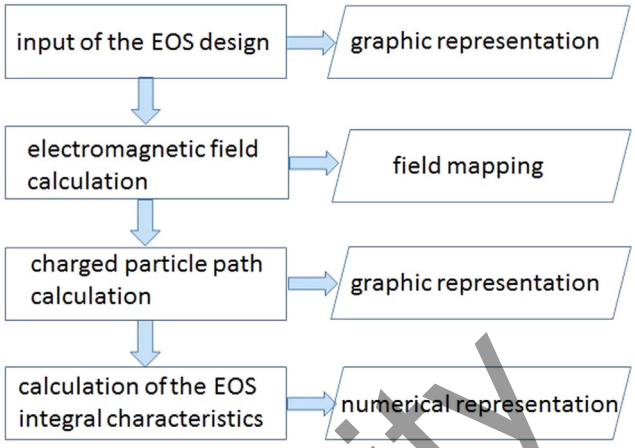


**Figure 4.** Block diagram of EOS numerical modeling.

## 3. Modeling Methods

### *3.1. Electron and Ion Optics Modeling Software "Focus"*

Numerical modeling of electron-optical systems (EOSs) traditionally includes the following consecutive steps (see Figure 4):

1. input of sizes and potentials of all electrodes of EOSs;
2. calculation of the electrostatic and magnetic fields, often by the finite difference method, or by finite element method, or by the boundary element method in the operational volume;
3. calculation of the trajectories of charged particles in the electromagnetic field of the system by the Runge–Kutta method;
4. computation of the integral characteristics of the EOS, such as angular focusing of a certain order, dispersion, resolution, aberration, distortion, etc., according to the results of calculations of the set of trajectories of charged particles.

To effectively solve the problems of numerical simulation of EOSs, the authors of this work developed the CAE "FOCUS" (Trubitsyn et al. 2017; Gurov et al. 2015). CAE "FOCUS" is in constant development—the algorithms of all steps of simulation are being improved in order to improve the accuracy and counting rate, and the functionality of the program is being expanded. The current version of the program includes the following calculation modules.

*The Design module* is a graphical editor. It is designed for the formation and modification of the EOS design. The cross section of the electrode system of each EOS can be represented by the union of the following primitives—a segment, a circular arc, a parabola, a hyperbola, a spline, a rectangle, and an ellipse. Each electrode of the system with its specified potential is a closed loop, which makes it possible to simulate designs with electrodes of finite thickness and arbitrary shape, i.e., designs as close as possible to real devices. Additionally, the module provides the possibility of three-dimensional representation of the simulating schemes.

At present, for the numerical solution of potential theory problems, three methods are widely used: the finite difference method, the finite element method, and the boundary element method (BEM).

The most advanced numerical methods for solving problems of mathematical physics that appeared in the computer era include the BEM (Wrobel & Aliabadi 2002). Its advantages include the simplicity of algorithm presentation and the possibility of solving both external and internal problems of the potential theory with an arbitrary boundary configuration (and with elements of different scales) of the study area.

Along with the obvious advantages, the BEM has a disadvantage, which is the singular behavior of integrand functions; this leads to an unacceptably high computational error. The development of an original numerical mathematical method (Trubitsyn 1995; Gurov et al. 2015) for excluding singularities from the integrand functions allowed BEM to be made into a powerful tool for calculation of electric fields in systems with an almost arbitrary boundary configuration and provided a level of calculation accuracy limited only by round-off errors.

The mathematical apparatus created for determination of the potential distribution function in the EOS by the boundary element method is the basis of the *Field_E* module of the "FOCUS" software.

In order to simulate magnetic fields, the *Field_M* module has been developed and integrated into the CAE "FOCUS". The module solves the problem of calculating the distribution function of the magnetic field induction of a set of solenoids by directly applying one of the basic laws of magnetostatics—the Biot–Savart law. The position of each solenoid in space is set by the coordinates of the center of its upper base and two angles that determine the orientation of its axis in space. The problem is solved by representing the resulting field as a superposition of magnetic fields of a set of solenoids, where the field of each of them, in turn, is defined as a superposition of magnetic fields of elementary circular currents (coils; Bimurzaev et al. 2021).

The *Path_S* module of CAE "FOCUS" is intended for express analysis of the trajectory of EOSs.

A more powerful set of user-defined functions and analytical capabilities is represented by another *Path_D* module for 3D trajectory analysis of systems with alternating electric and direct magnetic fields. The solution of the equations of motion of charged particles is carried out by the Runge–Kutta–Felberg method, which makes it possible to control the accuracy of the calculations.

Based on the results of the trajectory analysis of EOSs, the conditions for angular and time-of-flight focusing are automatically determined. Original numerical methods have been proposed and developed to search for focusing conditions (Trubitsyn 2001; Trubitsyn et al. 2010).

The developed mathematical methods and algorithms implemented in the CAE "Focus" were thoroughly tested according to standard methods. Based on a comparative analysis of the calculated data and known analytical solutions, it was established that the following characteristics can be achieved in real time:

—calculation of potentials (up to the area boundaries) with an accuracy not worse than $10^{-4}$%; in the case of rectilinear sections of electrodes in real time, the accuracy is limited only by round-off errors;

—calculation of particle trajectories with an accuracy not worse than $10^{-3}$%,

—calculation of parameters when searching for focusing conditions (angular, spatial, time-of-flight) not worse than $10^{-2}$%.

### 3.2. Original Numerical Method to Search for High-order Angular Focusing Conditions

The quality criterion for most electron and ion optics systems is the order of the angular focusing they provide.

The focusing condition of order $N$ is expressed by the equality of partial derivatives to zero with respect to the initial angle $\alpha$ in the meridian section $x0y$ according to the Taylor series:

$$y'(\alpha_0) = y''(\alpha_0) = \cdots = y^{(N)}(\alpha_0) = 0. \quad (1)$$

The coordinates $y$ of the trajectory intersect the focal plane:

$$y(\alpha) = y(\alpha_0) + (\partial y/\partial\alpha)_0\Delta\alpha + (1/2)(\partial^2 y/\partial\alpha^2)_0\Delta\alpha^2 + \cdots, \quad (2)$$

where $\Delta\alpha = \alpha - \alpha_0$, and $\alpha_0$ is the initial angle of the central trajectory.

The original numerical method to search for the angular focusing conditions of particle flows is described in sufficient detail in Trubitsyn (2001) and Gurov et al. (2015). The following is a brief summary of instructions for using the method.

On a discrete set of initial angles $\alpha_i$, $i = 1, 2, ..., L$ of particle motion in a certain selected range of angles $[\alpha_{\min}, \alpha_{\max}]$, a continuous function is constructed:

$$F(\alpha) = R''(\alpha)t'(\alpha) - R'(\alpha)t''(\alpha), \quad (3)$$

where $R(\alpha) = y_c(\alpha) + x_c(\alpha)t(\alpha)$, $t(\alpha) = \tan(\gamma)$; $\gamma(\alpha)$ and $x_c(\alpha)$, $y_c(\alpha)$ are the angle and coordinates at any convenient point of the final straight section of the trajectory. Derivatives are calculated using the formulae for numerical differentiation (Wolfe et al. 1966).

Then the algebraic equation

$$F(\alpha) = 0 \quad (4)$$

is solved with respect to $\alpha = \alpha_0$ and the coordinates of the focus point are determined by the formulae

$$x_0 = R'(\alpha_0)/t'(\alpha_0), \quad y_0 = R(\alpha_0) - x_0 \times t(\alpha_0). \quad (5)$$

To establish the angular focusing order, the cross-correlation of the function $F(\alpha)$ with the power function $S(\alpha) = (\alpha - \alpha_0)^{m+1}$ is estimated from the formula

$$\rho_0(m) = R_{FS}/(K_F \times K_S)^{1/2}, \quad (6)$$

with a sequential change in the value of $m = 0, 1, ..., M$ ($M$ is the upper search boundary). Here $R_{FS} = \frac{1}{L}\sum_{i=1}^{L}(F_i - \overline{F})(S_i - \overline{S})$, $K_F = \frac{1}{L}\sum_{i=1}^{L}(F_i - \overline{F})^2$, $K_S = \frac{1}{L}\sum_{i=1}^{L}(S_i - \overline{S})^2$, $\overline{F} = \frac{1}{L}\sum_{i=1}^{L}F_i$, and $\overline{S} = \frac{1}{L}\sum_{i=1}^{L}S_i$.

Next, the value of $m$ ($0 \leqslant m \leqslant M$) is determined for which $\rho_0(m) = \max\{\rho_0(0), \rho_0(1), ..., \rho_0(M)\}$. The proximity of $\rho_0(m)$ to 1 will indicate the mutual correlation of $F(\alpha)$ and $S(\alpha) = (\alpha - \alpha_0)^{N+1}$, i.e., focusing of the $N = m + 2$ order. The upper search limit $M$ is selected for practical reasons to be no more than 20–25.

### 3.3. Multipole Approach for Electrostatic Field Synthesis

Two-dimensional electrostatic multipoles with a rectilinear symmetry axis are well known and widely used as focusing, deflecting, and correcting elements in electron and ion optics. It is important to develop a multipole approach to solving the external Dirichlet problem in a cylindrical coordinate system (Zashkvara & Tyndyk 1996). It was shown (Zashkvara & Tyndyk 1999) that if on a cylindrical surface the potential and its first derivative with respect to the radial component are given by power series in the axial component, then the external field is the sum of circular multipoles. Based on this, new multipole-cylindrical fields were calculated, which are of interest for practical application in particle optics.

Axially symmetric electrostatic multipole-cylindrical fields are constructed on the basis of a superposition of a cylindrical field and circular multipoles of various orders, which were first considered by Zashkvara & Tyndyk (1992). In subsequent papers (Zashkvara et al. 2002; Saulebekov et al. 2011, 2019), the proposed approach was applied to study a family of multipole-cylindrical fields formed when the zero equipotential surface of a cylindrical field coincides with the zero equipotential surfaces of some circular multipoles. The considered axially symmetric fields have a simple structure and are promising for use in the mirror regime of reflection of a charged particle beam.

The class of multipole-cylindrical fields does not allow separation of variables in the equations of motion of charged particles, that is, it is impossible to obtain an analytical solution. The calculation of the trajectories by the numerical method, in comparison with the analytical one, significantly complicates the search for the condition of angular focusing of a charged particle beam. The method of analytical description of trajectories by an optimally selected superposition of power series describing the trajectory in the plane in integro-differential form and the condition for stitching the trajectory branches at its vertex is applied for quadrupole-cylindrical (Saulebekov et al. 2018), hexapole-cylindrical (Ashimbaeva et al. 2005), decapole-cylindrical (Kambarova et al. 2018), and octupole-cylindrical (Saulebekov et al. 2021) fields. Operating with finite sums of the additives that make up the power series, as shown in these works, makes it possible to describe the corpuscular-optical properties of systems with sufficient accuracy.

The potential of a hexapole-cylindrical field is described in the $r$, $z$ coordinate system by the following expression:

$$U(r, z) = \mu \ln r + \gamma U_h(r, z), \tag{7}$$

where

$$U_h(r, z) = \frac{1}{2}\left\{\ln r\left[z^2 - \frac{1}{2}r^2 - \frac{1}{2}\right] + \frac{1}{2}r^2 - \frac{1}{2}\right\} \tag{8}$$

is a circular hexapole, $\mu$ is the coefficient specifying the weight contribution of the cylindrical field $\ln r$, and $\gamma$ is the weight component of the circular hexapole.

The outer electrode, to which the deflection potential $U_o$ is applied, has a curved profile, the shape of which is determined by the equation

$$z = \pm\sqrt{\frac{4\frac{U(r,z)}{V} + \ln r\,(r^2 + 1 - \mu) - r^2 + 1}{2\cdot\ln r}}, \tag{9}$$

where $U(r, z)$ is the distribution of the hexapole-cylindrical field.

The energy analyzer scheme with a hexapole-cylindrical field for a cylindrical field component $\mu = 2$ and a circular hexapole $\gamma = 1$ is shown in Figure 5 (Ashimbaeva et al. 2006). The hexapole-cylindrical field is formed in the analyzer from two coaxial electrodes; the inner one remains cylindrical, and the outer electrode, which coincides with the equipotential of the hexapole-cylindrical field, has a curvilinear profile relative to the surface of the inner cylindrical electrode.

An approximate analytical approach to calculating the parameters of an analyzer with a hexapole-cylindrical field is as follows.

The distribution of a hexapole-cylindrical field in Equation (7) in coordinates $x$, $\xi$ (see Figure 5) has the following form:

$$U(x, \xi) = V \times g(x, \xi), \tag{10}$$

where

$$g(x, \xi) = \frac{1}{4}\{\ln(H - x)[2\xi^2 - (H - x)^2 + 7] + (H - x)^2 - 1\}, \quad H = 1 + \rho_m. \tag{11}$$

The basic trajectory of a particle in an electrostatic hexapole-cylindrical mirror has a vertex in the field area and, in the general case, is not described by an elementary function. This planar trajectory is called a "return" one. The "return" trajectory of charged particles consists of two branches that are symmetric with respect to the vertex. The integro-differential equation of motion of a charged particle along the "return" trajectory in the hexapole-cylindrical field has the following form:

$$(\xi')^2\left[g_0 - g_x - \int_0^x \ln(H - x)\,\xi\xi' dx\right] = P^2\cot^2\alpha_0 - f_m + \int_0^x \ln(H - x)\,\xi\,\xi' dx, \tag{12}$$

where

$$g_0 = g(x_m, \xi_m) = \ln H\left[-\frac{H^2}{4} + \frac{7}{4}\right] + \frac{H^2}{4} - \frac{1}{4}, \quad g_x = g[x, \xi(x)]. \tag{13}$$

and $P = \sqrt{(E_0/qV)\sin^2\alpha_0}$ is the reflection parameter linking the geometric and energy parameters of the mirror; $E_o$ and $q$ are the initial energy and charge of a particle, and $V$ is the potential of the deflection electrode.

To solve the integro-differential Equation (12), the expansion method of the solution of the equation, $\xi$, in a fractional power series is used:

$$\xi = \xi(x) = \sqrt{x}\,(C_0 + C_1 x + C_2 x^2 + C_3 x^3 + C_4 x^4 + C_5 x^5 + ...). \tag{14}$$

Having obtained the expansion of the derivative $\xi'$ in a series from Equation (14), and also using the expansion

$$\ln(H - x) = \ln H - \frac{x}{H} - \left(\frac{x}{H}\right)^2 - \left(\frac{x}{H}\right)^3 - \left(\frac{x}{H}\right)^4 - \left(\frac{x}{H}\right)^5 - ..., \tag{15}$$

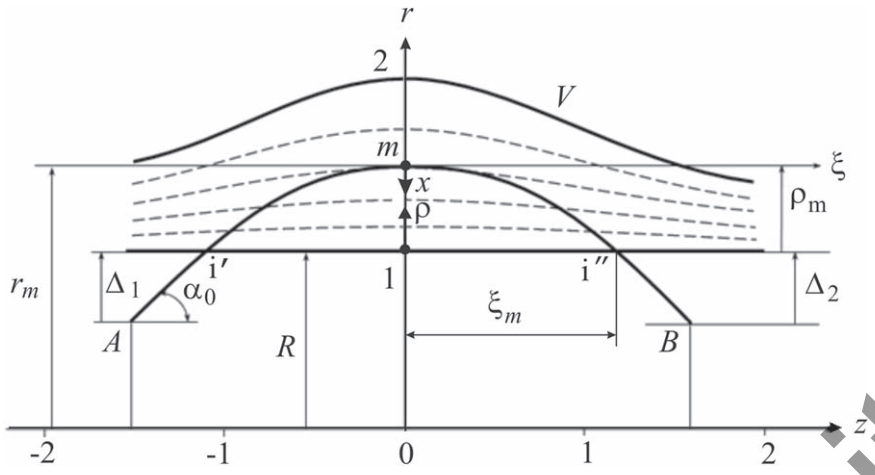


**Figure 5.** Energy analyzer scheme based on a hexapole-cylindrical field: i—source, i′—entrance ring slit, i″—exit ring slit, B—receiver.

**Table 1**
The Main Electron-optical Characteristics of the Hexapole-cylindrical Analyzer

| $P$ | $\alpha_o$ | $\rho_m$ | $\Delta$ | $\xi_m$ | $l$ | $D$ | $A_{\text{III}}$ | $\lvert\Delta l\rvert$ | $\delta$ |
|---|---|---|---|---|---|---|---|---|---|
| 0.10 | 30°165 | 0.005 | 0.010 | 0.0173 | 0.0518 | 0.0346 | −0.158 | 0.0009 | 27.95 |
| 0.50 | 33°922 | 0.130 | 0.264 | 0.400 | 1.193 | 0.849 | −2.809 | 0.0160 | 53.12 |
| 0.95 | 44°977 | 0.465 | 0.787 | 1.131 | 3.050 | 2.417 | −0.394 | 0.0061 | 385.26 |

it is possible to solve the integro-differential Equation (12) with respect to the unknown coefficients $C_0$, $C_1$, ..., i.e., to determine the trajectory of the particle $\xi = \xi(x)$ (see Equation (14)).

Below are the results of calculating the main parameters of the trajectory based on the analysis of the obtained solution.

The projection of the trajectory onto the $\rho$ axis from the entry point to the turning point has the expression

$$\rho_m = 0.5P^2 + 0.125\,P^4 + (0.013525 - 0.0625\cot^2\alpha_o)P^6 + \ldots. \quad (16)$$

The projection of the trajectory onto the symmetry axis of the mirror in the same section of motion is determined by the formula

$$\xi_m = \xi(x)|_{x=\rho_m} = \sqrt{\rho_m}\,C_o S, \quad (17)$$

where

$$C_o = \cot\alpha_o \times \sqrt{2.0P^2 + P^4 + 0.625P^6 + (0.52778 - 0.125\cot^2\alpha_o)\,P^8 + \ldots}, \quad (18)$$

$$S = 1 - 0.04167\,P^2 - (0.03073 + 0.02083\cot^2\alpha_o)\,P^4 - (0.02755 + 0.0092\cot^2\alpha_o)\,P^6 + \ldots. \quad (19)$$

Due to the symmetry of the "return" trajectory relative to the $r$ axis, the total projection of the trajectory onto the $z$-axis from source A to its image B, expressed in fractions of the radius $R$ of the inner cylinder, is the following sum:

$$l = \frac{L}{R} = \Delta\cot\alpha_0 + 2\xi_m,\ \Delta = \Delta_1 + \Delta_2. \quad (20)$$

To analyze the characteristics of an electrostatic hexapole-cylindrical energy analyzer, the spatial focusing coefficients of the first, second, and third orders were calculated: $\frac{dl}{d\alpha}$, $\frac{d^2l}{d\alpha^2}$, $\frac{d^3l}{d\alpha^3}$. The conditions for second-order angular focusing with respect to the small deviation of the nonequilibrium trajectory from the axial orbit are found: $\frac{dl}{d\alpha} = \frac{d^2l}{d\alpha^2} = 0$. The calculation of the specific energy dispersion is performed, which is a measure of the resolving ability at a small width of the ring slits A and B and is equal to the ratio of the linear energy dispersion to the width $s_0$ of the image line:

$$\delta = \frac{D}{s_0} = \frac{D}{A_{\text{III}} \times (\Delta\alpha)^3}, \quad (21)$$

where $D = \frac{\partial l}{\partial E}E_0$ is the value of the relative linear energy dispersion and $A_{\text{III}} = \frac{1}{3!}\frac{d^3l}{d\alpha^3}$ is cubic angular aberration.

Table 1 presents a small example, which shows the main electron-optical characteristics of the analyzer, calculated as a function of the reflection parameter $P$ and satisfying the conditions of second-order angular focusing: $\alpha_o$ is the entrance angle of the trajectory; $\rho_m$ is the coordinate of the trajectory vertex point in the mirror field; $\Delta = \Delta_1 + \Delta_2$ is the value of the total distance of the source and its image from the inner cylindrical electrode; $\xi_m$ is a half projection of the trajectory onto the symmetry axis in the mirror field; $l$ is a focal length; $D$ is the value of relative linear energy dispersion; $A_{\text{III}}$ is the cubic angular aberration; $\Delta l$ is the value of the aberrational image expansion; and $\delta$ is the value of the specific energy dispersion.

## 4. Modeling the Entrance Optics of the Spectrometer

Based on the results of numerical calculations, the design of an entrance lens system is proposed that converts the flow of charged particles emitted from different points of the celestial hemisphere into a narrow hollow conical beam (Figure 6). The electrodes of the lens system are formed by the simplest, and therefore technologically advanced, primitives—disks, cylinders, and cones.

Charged particles (1) (Figure 6) with energy $E_0$ ($E_0/V = 1$), emitted by sources distributed in some way over the surface of

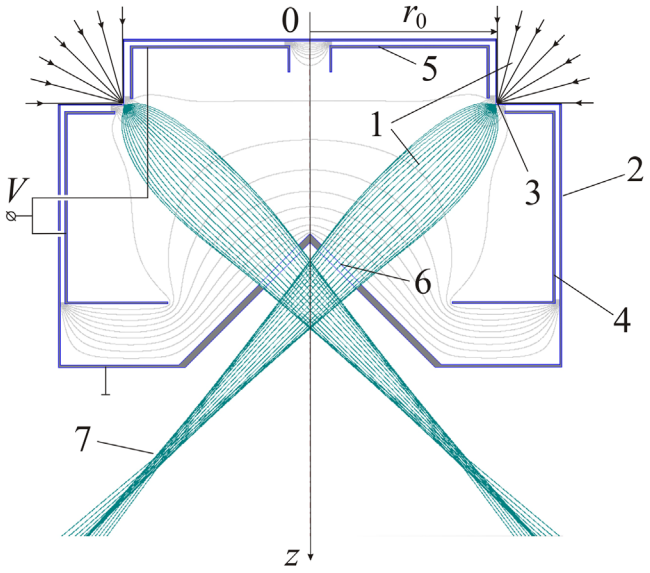


**Figure 6.** The meridional section of the entrance lens system of a simple design with a full view of the celestial hemisphere: 1—particle flow, 2—device body (an outer electrode), 3—entrance ring diaphragm, 4, 5—inner U-shaped electrodes, 6—exit window, 7—focal point.

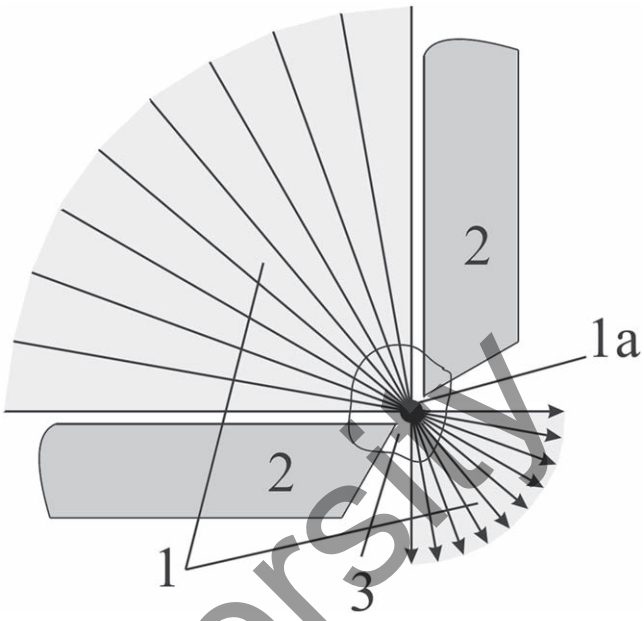


**Figure 7.** Scheme of particle flow passing through the entrance ring diaphragm (transaxial section): 1—charged particle beam, 1a—virtual source, 2—the device body, 3—ring diaphragm.

the hemisphere of the sky with a large radius, moving along radial trajectories in the direction of the device body (2), penetrate through the entrance ring diaphragm (3) (see Figure 7) into the field of a single conical electrostatic lens, formed by a zero potential on the outer electrode (2) and potentials $V$ on the inner electrodes (4 and 5) of the U-shaped section, applied from an external power source. The flow (1), having experienced the focusing effect of this field, enters the external space through a window (6) covered with a fine-structured metal mesh in the conical surface of the outer electrode (2), forming a hollow narrow collimated truncated cone with a smaller base located in the focal region (7).

A detailed numerical analysis of the scheme of the lens system (Figure 6) shows that a single conical lens is represented by two areas, which play the role of successive short-focus and long-focus collecting lenses.

Figure 8 shows the effect of parallel beam focusing by the first collecting lens with an initial relative electron energy $E/V = 1$. The initial angle of entry of a parallel charged particle beam into the lens field is −45° with respect to the $0z$ symmetry axis. The focal length, which is calculated from the center of the entrance diaphragm (3), is $f_1 = 0.15r_0$. In the modeling, the outer electrode was considered transparent to the particle beam.

In the case of emission of a divergent flow by a thin ring source 1a (Figure 7) located in the area of the entrance diaphragm 3, after transit through the first lens, charged particles enter the area of the second lens in an almost parallel flow perpendicular to the equipotential of $0.7V$ and therefore are collected at the focus 7 of this lens (see Figure 6).

The exact estimate of the distance from source 3 to image 7 (Figure 6), obtained in accordance with numerical calculations, is about $3.3r_0$; this provides the second-order angular focusing near the central angle of 45°.

## 5. Modeling of the Second Stage of the Spectrometer

The second stage of the analyzer is to ensure the spatial separation of the moving ions in terms of energy and the

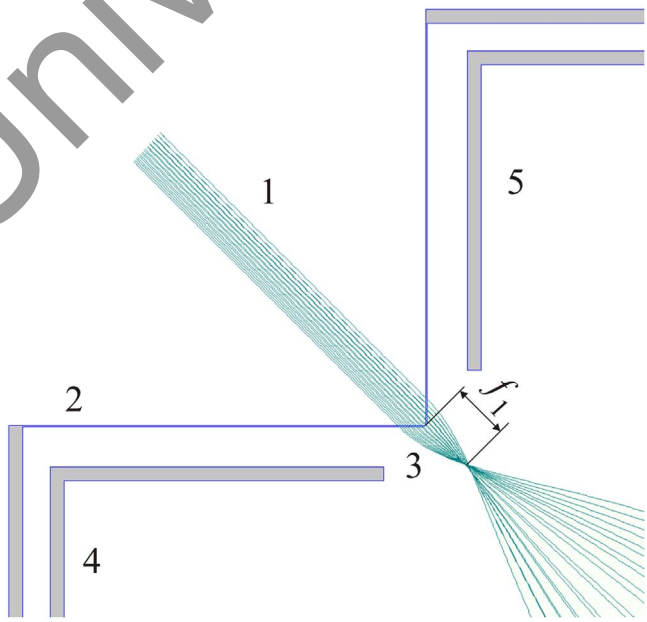


**Figure 8.** Entrance collecting lens: 1—particle beam, 2—the device body (an outer electrode), 3—the entrance ring diaphragm, 4, 5—inner U-shaped electrodes.

angular focusing of the ion flow at the exit slit. The ability of the device to separate particles by energy is characterized by the value of the energy dispersion, and its focusing qualities are determined by the angular focusing order. The central angle of departure from the first stage of the device is approximately 45°; therefore, the second stage must have a high angular focusing order (higher than the first one) relative to the trajectory of a particle with such an initial angle. A wide range of second-order focusing angles within 30°–50° and a number of other unique electron-optical characteristics are provided by designs of devices with hexapole-cylindrical fields $U(r, z) = \mu \ln r + \gamma U_h(r, z)$ (see Section 3.3). From the analysis of the

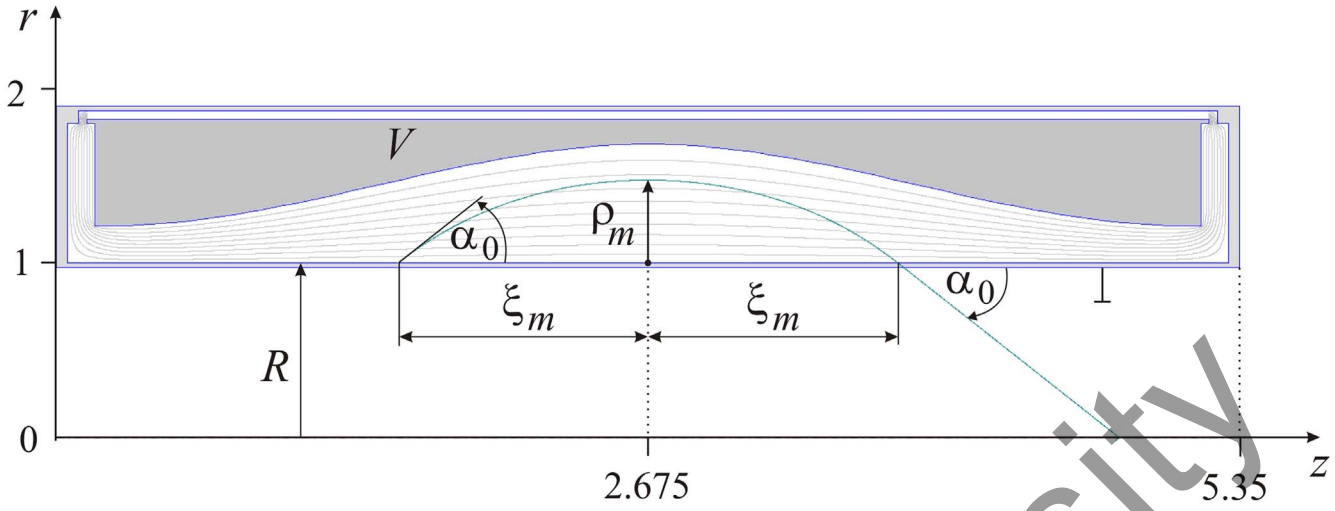


**Figure 9.** The electron-optical scheme of the second stage of the analyzer: $R = 1$.

calculated data of Ashimbaeva et al. (2006), it follows that the required angle of 45° can be obtained in the scheme with $\mu = 2$ and $\gamma = 1$. Examples of theoretically calculated parameters of the analyzer of this scheme are presented in Table 1.

The case of $P = 0.95$ satisfies the conditions of the problem solved in the article. In addition, this scheme is distinguished by a high level of specific energy dispersion $\delta = 385.26$, which is approximately six times higher than the specific dispersion of a cylindrical mirror analyzer, having $\delta = 65.5$ for a better "axis–axis" focusing scheme. Another advantage of the scheme is the small value of the third-order angular aberration $A_{III}$, which guarantees a narrow focus of highly divergent particle flows.

The characteristics presented in Table 1 were calculated for electrodes of infinite length along the $z$-axis. In a real device, the length of the electrodes must be limited. With limited length, the influence of edge effects can be neglected if the places where the electrode shape is distorted are located at a considerable distance from the particle transit area. Figure 9 shows the electron-optical scheme of the hexapole-cylindrical analyzer of real dimensions, as well as the central trajectory of a particle with initial conditions corresponding to the regime of $P = 0.95$ in Table 1: the initial angle $\alpha_0 = 44.9774°$ and the relative initial energy $\frac{E_0}{V} = \left(\frac{P}{\sin\alpha_0}\right)^2 = \left(\frac{0.95}{\sin 44.9774°}\right)^2 \approx 1.806$. Table 2 compares the main characteristics of the calculated trajectories (Table 1) numerically and analytically. The results of the comparison show a high degree of agreement of the parameters of the idealized and real schemes. From the above, the conclusion is drawn that the hexapole-cylindrical analyzer can be considered as the second stage of the designed device.

Indeed, the trajectory analysis of the second hexapole-cylindrical stage, when the particles that left the first stage are launched to its entrance (Figure 6), reveals rather sharp angular focusing (of second order) near 45° to the initial particle beam. Note that the polar angles were spread within the range from 0° to 90° at the entrance to the first stage. In the modeling, the first and second stages are matched along the central trajectory of a particle entering the second one at a distance of $\xi_m$ from the top of the outer electrode (Figure 10).

**Table 2**
Comparison of the Main Electron-optical Characteristics of the Second Stage Calculated Analytically (Idealized Scheme, Figure 5) and Numerically (Real Scheme, Figure 9)

| Parameter | $P$ | $\alpha_o$ | $\rho_m$ | $\xi_m$ | $D$ |
|---|---|---|---|---|---|
| Idealized scheme | 0.950 | 44.°977 | 0.465 | 1.131 | 2.417 |
| Real scheme | 0.946 | 44.°980 | 0.475 | 1.131 | 2.027 |

## 6. Modeling of the Energy and Angular Dependences of the Spectrometer

The electron-optical scheme and the results of the trajectory analysis of the entire device as a sequence of two stages are shown in Figure 10. The scheme of the device provides the second-order angular focusing near the trajectory $\alpha_0 = 44.9°$ in the meridional section with coordinates $z = 19.9$, $r = 1.45$. The design of the device includes a narrow entrance ring slit (1), the first-stage exit window (2), entrance (3) and exit (4) windows of the second stage, and entrance (5) and exit (6) ring-shaped limiting diaphragms. Windows 2, 3, and 4 are tightened with a fine-structured metal mesh, preventing potential sag and providing charged particle transit. Ring-shaped diaphragms (5 and 6) are located in the smallest section of the particle flow. The potential of the first-stage focusing electrodes is $V_1 = V = E_0$[eV] and the potential of the second-stage outer electrode is $V_2 = 0.556V = 0.556E_0$[eV], where $V$ is the voltage of the external power source and $E_0$[eV] is the particle energy in eV.

Figure 11 shows the instrumental function of the energy analyzer, which is the dependence of the relative number of particles $N/N_0$ registered by the collector on the relative energy $E_0/V$. The half-height resolution is $R_{\mathrm{FWHM}} = \Delta E_{\mathrm{FWHM}}/E_0 = 1.1\%$, and the luminosity is $\Omega \approx 100\%$ of $2\pi$. Here, $\Delta E_{\mathrm{FWHM}}$ is the full energy width at half-maximum of the instrumental function.

Each polar angle $\alpha$ of the celestial sphere corresponds to a circle of a certain radius on the surface of the plane coordinate-sensitive detector (7) (Figure 10). Furthermore, each point of this circle determines the azimuthal direction $\theta$ to the particle source within the range from 0 to $2\pi$. Thus, the angular

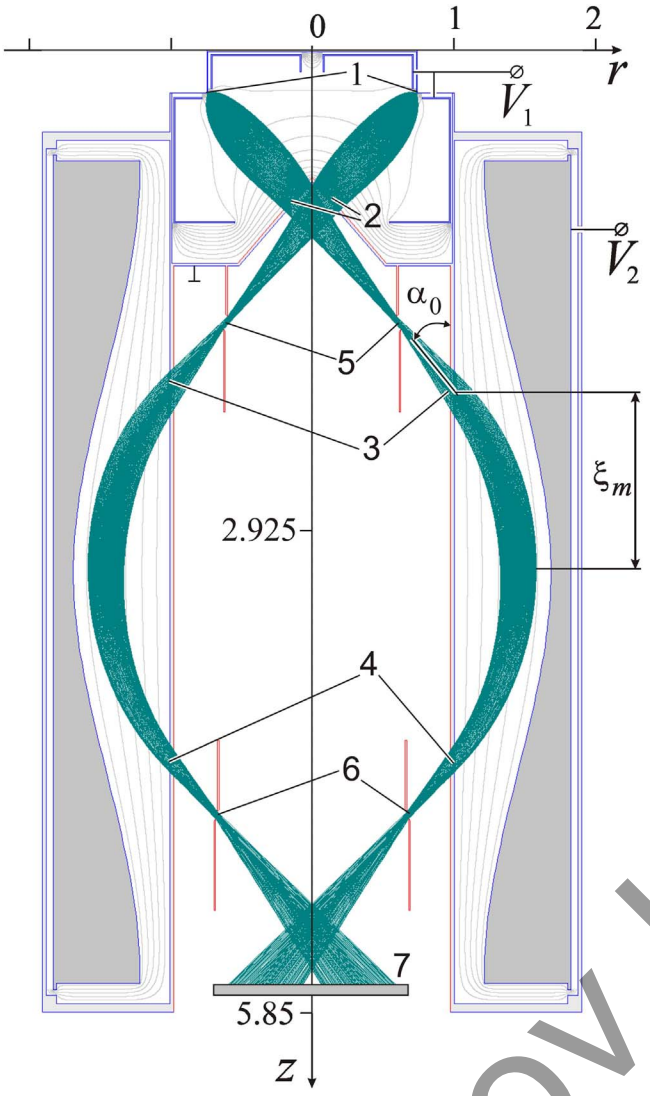


**Figure 10.** The electron-optical scheme of the all-sky spectrometer of hot cosmic plasma: $E_0/V_1 = 1$, $E_0/V_2 \approx 1.8$.

resolution of the device is determined by the spatial resolution of the position-sensitive detector used. The trajectory analysis of the design in Figure 10 made it possible to establish the average value of $\frac{1}{R}\frac{\Delta r}{\Delta\alpha}$ in the plane of the detector located at a distance of $5.675R$ from the source, which turned out to be 0.005. Therefore, the polar angle resolution can be determined by the formula $\Delta\alpha = \frac{\Delta p}{0.005R}$, where $\Delta p$ is the spatial resolution of the detector. The azimuthal angle resolution is evaluated in accordance with the fairly obvious relation $\Delta\theta = \frac{\Delta p}{r_{\rm in}}\frac{180^\circ}{\pi}$, where $r_{\rm in}$ is the inner (smaller) radius of the image ring on the detector plane. For the developed scheme (see Figure 10), the value of $r_{\rm in} \approx 0.1R$. As a position-sensitive detector for the developed spectrometer, an Si pixel detector fits perfectly, for example, from ADVACAM[4] (2022), whose standard pixel pitch is 55 $\mu$m, i.e., with $\Delta p = 55 \times 10^{-6}$ m. In the case of a specific version of the device, for example, with a radius of the inner cylinder $R = 50$ mm, when using the ADVACAM detector, the parameters of the angular resolution will reach the following values: $\Delta\alpha \approx 0.^\circ 2$, $\Delta\theta \approx 0.^\circ 7$. If necessary, the

[4] https://advacam.com/camera

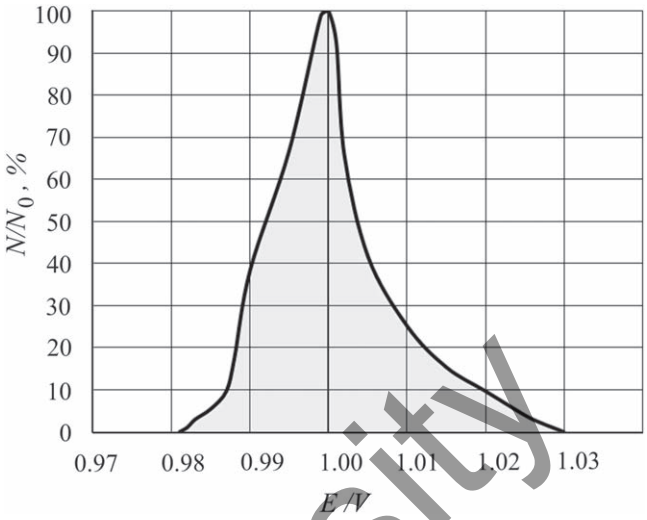


**Figure 11.** The instrumental function of the spectrometer.

angular resolution can be improved, particularly when using detectors of the Adva*PIX* TPX3 type from ADVACAM Company. Recording individual hits together with advanced data processing allows imaging at super spatial resolution $\Delta p$. In some applications it can reach units of microns (X-rays) or even a sub-micrometric level (ions).

To estimate the spectrometer sensitivity, we calculate the effective area of the entrance slit (Figure 10). When estimating, we will use the dimensions of the analyzer apertures according to the results of trajectory analysis (see Figure 10) with the calculated energy resolution $R_{\rm FWHM} = 1.1\%$ (Figure 11). In accordance with Liouville's theorem, the phase volume of an ensemble of particles remains unchanged when moving in space. If the particle energy does not change, then the product of the area $S$ of the beam cross section and the corresponding solid angle $\Omega$ is preserved. At the point of passage of the section of the entrance diaphragm 5 (Figure 10), we have the opportunity to estimate the value of such a product (geometric factor) $G = S \times \Omega$, taking into account the fact that in this section the area of the ring diaphragm 5 with width $\Delta z \approx 0.08R$ is equal to $S \approx 2\pi \times 0.61R \times \Delta z = 2\pi \times 0.049R^2$ and $\Omega \approx 2\pi(\cos 35^\circ - \cos 50^\circ) = 2\pi \times 0.18$ sr, i.e., $G \approx 4\pi^2 \times 0.0086R^2$. From here it is possible to determine the effective area of the entrance slit of the spectrometer as $S_{\rm eff} = G/2\pi = 0.054R^2$. In this case, with an entrance slit radius of approximately $0.7R$, its effective width will be $\Delta r \approx S_{\rm eff}/(2\pi \times 0.7R) \approx 0.011R$. For a device with an inner cylinder radius $R = 50$ mm, the parameters under consideration will take the specific values $S_{\rm eff} \approx 135$ mm$^2 \approx 1$ cm$^2$ and $\Delta r \approx 0.6$ mm. Known values of the ion flow density in the slow solar wind ($3.9 \times 10^8$ cm$^{-2}$ s$^{-1}$) and in the fast solar wind ($2.7 \times 10^8$ cm$^{-2}$ s$^{-1}$), as well as the average value of the flow density ($3.8 \times 10^8$ cm$^{-2}$ s$^{-1}$), allow particle fluxes to be measured (at spectrometer resolution $R_{\rm FWHM} = 1.1\%$) from the elementary product of these densities and $S_{\rm eff} \approx 1$ cm$^2$.

## 7. Conclusions

The two-stage, fairly simple design of the all-sky spectrometer of hot cosmic plasma is proposed in this work. The first stage of the device is the axially symmetric lens system of an original design, which transforms a wide $2\pi$ sr entrance particle beam into a narrow one in the form of a hollow cone.

The second stage, a hexapole-cylindrical one, serves as an energy analyzer of the beam. Using numerical and approximate analytical methods, the electron-optical scheme of the device, setting the second-order angular focusing regime, is developed. As a position-sensitive detector for the developed spectrometer, modern ones, for example, Si pixel detectors from ADVACAM Company, can be used.

In the next phase of research, it is planned to develop a 3D model of the device, create a prototype of the proposed analyzer, and carry out test trials.

The research was supported by the Ministry of Education and Science of the Republic of Kazakhstan, grant No. AP09058188.

## ORCID iDs

Zh. T. Kambarova https://orcid.org/0000-0001-9808-5484

## References

ADVACAM 2022, Company's product catalog: advacam.com/camera
Allegrini, G. F., McComas, D. J., & Louarn, P. 2016, JGRA, 121, 5121
Andrews, G. B., Zurbuchen, T. H., Mauk, B. H., et al. 2007, SSRv, 131, 523
Ashimbaeva, B. U., Chokin, K. S., & Saulebekov, A. O. 2005, J. Electron Spect. Rel. Phen., 143, 29
Ashimbaeva, B. U., Masyagin, B. E., Saulebekov, A. O., et al. 2006, Eurasian Phys. Techn. J, 3, 51
Becker, J. 2013, PhD thesis, UPMC, Paris
Bimurzaev, S., Sautbekova, Z., & Trubitsyn, A. 2021, in IEEE Intern. Conf. on SIST (New York: IEEE), 1
Collinson, A. G., Chornay, D. J., Glocer, A., et al. 2018, Rev. Sci. Instrum, 89, 113306
Collinson, G. A., McFadden, J. P., Chornay, D., et al. 2016, JGRA, 121, 7887
Fernandes, P. A., & Lynch, K. A. 2016, JGRA, 121, 7316
Gurov, V. S., Saulebekov, A. O., & Trubitsyn, A. A. 2015, in Analytical, Approximate-Analytical and Numerical Methods in the Design of Energy Analyzers, Adv. Imag. Electron Phys., ed. P. W. Hawkes (Amsterdam: Elsevier), 209
Kambarova, Zh.T., Trubitsyn, A. A., & Saulebekov, A. O. 2018, TePhl, 63, 1667
Kazama, Y. 2013, in An Introduction to Space Instrumentation, ed. C. Z. Cheng & K. Oyama (Tokyo: Terrapub), 181
Li, C., Wang, Y., Zhang, H., et al. 2018, J. Instrum., 13, 12027
Machida, S., Saito, Y., Ito, Y., & Hayakawa, H. 1998, EPS, 50, 207
Neugebauer, M., & Snyder, C. W. 1962, Sci, 138, 1095
O'Brien, B. J., Abney, F., Burch, J., et al. 1967, Rev. Sci. Instrum, 38, 1058
Paschmann, G., Loidl, H., Obermayer, P., et al. 1985, IEEE Trans. Geosc. Remote Sens, 23, 262
Saulebekov, A. O., Kambarova, Z. T., et al. 2021, Eurasian Phys. Techn. J., 18, 96
Saulebekov, A. O., Kambarova, Z. T., Trubitsyn, A. A., & Saulebekova, D. A. 2018, Eurasian Phys. Techn. J, 15, 35
Saulebekov, A. O., Trubitsyn, A. A., & Kambarova, Z. T. 2011, Bulletin of the University of Karaganda-physics, 1, 37
Saulebekov, A. O., Trubitsyn, A. A., & Kambarova, Z. T. 2019, Bulletin of the University of Karaganda-physics, 1, 87
Trubitsyn, A. 2001, Techn. Phys, 46, 630
Trubitsyn, A., Astakhov, V., & Grachev, E. 2010, in Eighth Intern. Conf. on CPO-8, 186
Trubitsyn, A., Grachev, E., Gurov, V., et al. 2017, Proc. SPIE, 10250, 102500V
Trubitsyn, A. A. 1995, Comp. Maths Math. Phys., 35, 421
Vaisberg, O. L. 2003, AdSpR, 32, 385
Vaisberg, O. L., Berthellier, J. J., Moore, T., et al. 2016, JGRA, 121, 11750
Vaisberg, O. L., Leibov, A. V., Smirnov, V. N., et al. 2006, Cosmic Res, 44, 202
Vaisberg, O. L., Koinash, G. V., Moiseev, P. P., et al. 2010, Solar Syst. Res., 44, 456
Victor, A. L., Zurbuchen, T. H., & Gallimore, A. D. 2006, Rev. Sci. Instrum., 77, 013505
Wolfe, J. H., Silva, R. W., McKibbin, D. D., & Mason, R. H. 1966, JGR, 71, 3329
Wrobel, L. C., & Aliabadi, M. H. 2002, The Boundary Element Method (New York: Wiley),
Zashkvara, V. V., Ashimbaeva, B. U., & Chokin, K. S. 2002, J. Electron Spect. Rel. Phen., 122, 195
Zashkvara, V. V., & Tyndyk, N. N. 1992, Nucl. Instrum. Meth. Phys. Res., A313, 315
Zashkvara, V. V., & Tyndyk, N. N. 1996, Nucl. Instrum. Meth. Phys. Res., A370, 452
Zashkvara, V. V., & Tyndyk, N. N. 1999, Nucl. Instrum. Meth. Phys. Res., A370, 223